Astronomy & Astrophysics

Detection of HCN, HCO+, and HNC in the Mrk 231 molecular outflow[*]

Dense molecular gas in the AGN wind

S. Aalto[1], S. Garcia-Burillo[2], S. Muller[1], J. M. Winters[3], P. van der Werf[4], C. Henkel[5,6], F. Costagliola[1], and R. Neri[3]

[1] Department of Earth and Space Sciences, Chalmers University of Technology, Onsala Observatory, 439 94 Onsala, Sweden
e-mail: saalto@chalmers.se
[2] Observatorio Astronómico Nacional (OAN)-Observatorio de Madrid, Alfonso XII 3, 28014-Madrid, Spain
[3] Institut de Radio Astronomie Millimétrique (IRAM), 300 rue de la Piscine, Domaine Universitaire de Grenoble, 38406 St. Martin d'Hères, France
[4] Leiden Observatory, Leiden University, 2300 RA, Leiden, The Netherlands
[5] Max-Planck-Institut für Radioastronomie, Auf dem Hügel 69, 53121 Bonn, Germany
[6] Astronomy Department, King Abdulaziz University, PO Box 80203 Jeddah 21589, Saudi Arabia

ABSTRACT

Aims. Our goal is to study gas properties in large-scale molecular outflows and winds from active galactic nuclei (AGNs) and starburst galaxies.
Methods. We obtained high-resolution ($1\rlap.''55 \times 1\rlap.''28$) observations of HCN, HCO+, HNC 1–0 and HC$_3$N 10–9 of the ultraluminous galaxy (ULIRG) Mrk 231 with the IRAM Plateau de Bure Interferometer.
Results. We detect luminous emission from HCN, HCO+ and HNC 1–0 in the QSO ULIRG Mrk 231. All three lines show broad line wings - which are particularly prominent for HCN. Velocities are found to be similar ($\approx\pm750$ km s^{-1}) to those found for CO 1–0. This is the first time bright HCN, HCO+ and HNC emission has been detected in a large-scale galactic outflow. We find that both the blue- and red-shifted line wings are spatially extended by at least $0\rlap.''75$ (>700 pc) in a north-south direction. The line wings are brighter (relative to the line center intensity) in HCN than in CO 1–0 and line ratios suggest that the molecular outflow consists of dense ($n > 10^4$ cm^{-3}) and clumpy gas with a high HCN abundance X(HCN) $> 10^{-8}$. These properties are consistent with the molecular gas being compressed and fragmented by shocks in the outflow. Alternatively, HCN is instead pumped by mid-IR continuum, but we propose that this effect is not strong for the spatially extended outflowing gas. In addition, we find that the rotation of the main disk, in east-west direction, is also evident in the HCN, HCO+ and HNC line emission. An unexpectedly bright HC$_3$N 10–9 line is detected inside the central 400 pc of Mrk 231. This HC$_3$N emission may emerge from a shielded, dust-enshrouded region within the inner 40-50 pc where the gas is heated to high temperatures (200–300 K) by the AGN.

Key words. galaxies: evolution – galaxies: individual: Mrk 231 – galaxies: active – quasars: general – radio lines: ISM – ISM: molecules

1. Introduction

Mergers and interactions between galaxies trigger massive starbursts and feed the growth of supermassive black holes (SMBH) in their centers. Powerful outflows have been proposed to regulate both star-formation and the SMBH growth through negative feedback in young galaxies (e.g. Hopkins et al. 2009; Murray et al. 2005). Murray et al. (2005) suggest that momentum-driven winds and outflows are the underlying mechanism behind the Faber-Jackson relation for large elliptical galaxies.

In the past years, few studies have targeted outflowing molecular gas (e.g. Nakai et al. 1987; García-Burillo et al. 2001; Walter et al. 2002; Sakamoto et al. 2006) but recently evidence is mounting for massive molecular outflows in AGNs and starburst galaxies (Sakamoto et al. 2010; Feruglio et al. 2010; Fischer et al. 2010; Chung et al. 2011; Alatalo et al. 2011; Sturm et al. 2011) and high-velocity molecular outflows have been found in

OH-megamasers (e.g. Baan 2007). It is important to study outflowing molecular gas because this process removes gas immediately available for star formation from the galaxy, which impacts the evolution of the galaxy on short time scales. Furthermore, the molecular gas properties hold important clues to the nature and evolution of the outflow. Simulations of molecular cloud properties in galactic outflows have been carried out by e.g. Narayanan et al. (2008).

The ultraluminous infrared galaxy (ULIRG, log($L_{\rm IR}$) = 12.37) Mrk 231 is often referred to as the closest infrared quasar (QSO). It is a major merger and hosts powerful AGN activity as well as a young, dusty starburst with an extreme star-formation rate of ≈200 $M_\odot$ yr^{-1} (Taylor et al. 1999; Gallagher et al. 2002; Lipari et al. 2009). Massive amounts of molecular gas reside in an east-west rotating disk (Bryant & Scoville 1996; Downes & Solomon 1998). Radio continuum observations show jets and outflows ranging from pc to kpc-scale (Carilli et al. 1998; Lonsdale et al. 2003). Rupke & Veilleux (2011) discuss the various outflows of Mrk 231, and using high-resolution-spectroscopy, they describe a wide, kpc-scale, high-velocity

($\approx$1000 km s^{-1}) outflow seen in neutral gas (Na I D) absorption. Furthermore, they find that north of the nucleus the radio continuum jet is accelerating the outflow to even higher velocities ($\approx$1400 km s^{-1}) and 3.5 kpc south of the nucleus a slower, starburst-driven wind is found. They suggest that the high mass outflow rate of Mrk 231 (which is 2.5 times greater than the star-formation rate) is a result of the negative feedback from the AGN. Interestingly, the outflow has been detected in molecular gas in OH absorption (with velocities >1000 km s^{-1}) (Fischer et al. 2010) and also manifested in broad (750 km s^{-1}) wings in the CO 1–0 emission line (Feruglio et al. 2010). These authors estimate the outflow of molecular gas to 700 $M_{\odot}$ yr^{-1}, which could empty the reservoir of molecular gas within 10 Myr.

Feruglio et al. (2010) argue that the kinetic energy from the supernovae induced by the circumnuclear starburst disk is not sufficient to expel the gas and that action from the AGN is required. Furthermore, Murray et al. (2005) find that the mass loss rate in a starburst-driven outflow does not significantly exceed the star-formation rate (following their Eq. (13)). The high mass outflow rates of Feruglio et al. (2010) and Rupke & Veilleux (2011) seem to support the notion of an AGN-driven outflow. This conclusion is disputed by Chung et al. (2011), who find high-speed (1000–2000 km s^{-1}) molecular outflows in ULIRGs and argue that they can be powered by starbursts. They suggest that the mass outflow rate of Mrk 231 is overestimated if the CO emission in the outflow is optically thin. Clearly, a more detailed study of the properties of the gas in the outflow is essential for a better estimate of the mass in the outflow, but also to understand how the molecular gas is carried out of the galaxy and by what process. Is the molecular gas entrained in outflowing hot material – or is it being expelled by radiation pressure from an AGN and/or the momentum flux by supernovae? How can the the gas survive in molecular form – and for how long?

In our IRAM 30 m 3 mm EMIR spectrum (Costagliola et al. 2011) of Mrk 231 we found that the HCN and HCO$^+$ line widths were surprisingly broad, leading us to suspect that the outflow signature of Mrk 231 could be even more powerful in the rotational transitions of these high-density tracers. To confirm this discovery and to map the extent of the line emission, we asked for IRAM Plateau de Bure DDT time to observe HCN, HCO$^+$ and HNC in the B-array.

In Sects. 2 and 3 the observations and their results – bright HCN, HCO$^+$ and HNC 1–0 emission in the outflow line wings and a serendipitous detection of the HC$_3$N 10–9 line – are described. In Sects. 3.1 and 3.1 we discuss the spatial extent of the line wings, and in Sects. 4.1 and 4.2 potential underlying causes for the enhanced wing emission are outlined. Outflow gas properties and the nature of the outflow are discussed in Sect. 4.3. In Sect. 4.4 we discuss the origin of the HC$_3$N line emission, and finally in Sect. 4.5 a brief future outlook is outlined.

2. Observations

The observations were carried out with the six-element IRAM Plateau de Bure array on March 8, 2011, in B-array. The phase center was set to α = 12:56:14.232 and δ = 56:52:25.207 (J2000). Mrk 231 was observed for hour angles 2 (i.e. starting 2 hrs after source culmination) to 5 and the radio seeing was 0$''$8. The receivers were tuned to a frequency of 85.3125 GHz, the center between the two red-shifted line frequencies for HCN (ν = 85.046 GHz) and HCO$^+$ (ν = 85.579 GHz). Zero velocity refers to the redshift z = 0.042170 (Carilli et al. 1998) throughout the paper, resulting in a spatial scale of 1$''$ = 870 pc. We used the WideX correlator, which provides a broad frequency

range of 3.6 GHz, which also included the HNC 1–0 and HC$_3$N 10–9 lines.

The bandpass of the individual antennas was derived from the bright quasar 3C273. The flux calibration was set on 3C273. The close-by quasars J1259 + 516 ($\sim$0.32 Jy at 3 mm) and J1300 + 580 ($\sim$0.19 Jy) were observed regularly every 25 minutes for complex gain calibration.

After calibration within the GILDAS reduction package, the visibility set was converted into FITS format, and imported into the GILDAS/MAPPING and AIPS packages for additional imaging. Data were rebinned to 20 MHz (68 km s^{-1}) and cleaned with a robust weighting of 3, resulting in a beam size of 1$''$55$\times$1$''$28 and position angle PA = 57$°$. The corresponding rms noise is 0.48 mJy channel^{-1}.

3. Results

3.1. HCN

Spectra of all four detected lines are presented in Fig. 1. Prominent line wings are detected in the HCN 1–0 line out to velocities of 750 km s^{-1}, similar to those found in CO 1–0 by Feruglio et al. (2010). If we define the line-center-to-wings ratio (LCW) as the ratio between peak intensity at zero velocity to the intensity at +500 km s^{-1} in the red-shifted line wings, then the LCW for HCN 1–0 is 27 mJy/3 mJy = 9. In the CO 1–0 spectrum of Feruglio et al. (2010) the LCW is 320 mJy/8 mJy = 40. Another way of defining the LCW is to adopt the Gaussian fits in Fig. 1 of Feruglio et al. (2010), where two components, one with $\delta V(FWHM)$ = 180 km s^{-1} and one with $\delta V(FWHM)$ = 870 km s^{-1}, are fitted to the line center and outflow respectively. Fixing the linewidths of the two Gaussian componets to our data (see Fig. 3 for the Gaussian fit), we find an LCW for HCN of 7.7 and for CO 1–0 we estimate an LCW of 20.6.

Because the line wings are most prominent for HCN, we elected to show the line integrated intensity of the wings for this molecule only. The HCN 1–0 integrated intensity maps of the line wings and the total line emission are presented in Fig. 3, peak- and integrated intensities in Table 1. The total line emission is beginning to be resolved in the 1$''$55$\times$1$''$28 beam with features extending out to the west and northeast. These are generally consistent with similar features in the CO 2–1 map by Downes & Solomon (1998) and in the HCO$^+$ 4–3 map by Wilson et al. (2008). The central velocity gradient from the main disk is evident in HCN – showing the $\pm$150 km s^{-1} gradient seen in CO (Downes & Solomon 1998). The HCN 1–0 velocity field of the central component (wings excluded) is presented in Fig. 4. HCN position velocity diagrams along the rotational axis (PA = 90$°$) and along the wings (PA = 0$°$) are presented in Fig. 5.

3.1.1. Position of line wings and continuum subtraction

Because the line wings are broad and relatively faint, the determination of their positions depends on a reliable continuum subtraction. We used two methods of subtracting the continuum to test the relative errors in the wing position: subtraction in the uv-plane and in the image plane. The continuum was subtracted with a zeroth or first order fit to the line-free spectral channels. In general we find that the uncertainty in the wing peak position is 0$''$4. The continuum map is presented in Fig. 2. A Gaussian fit to the continuum source gives a flux density of 25.0 $\pm$ 0.6 mJy and an upper limit to the source size of 0$''$39.

The blue- and red-shifted HCN line-wings appear shifted by 0$''$2–0$''$4 (175–350 pc) to the southwest of the nucleus as defined
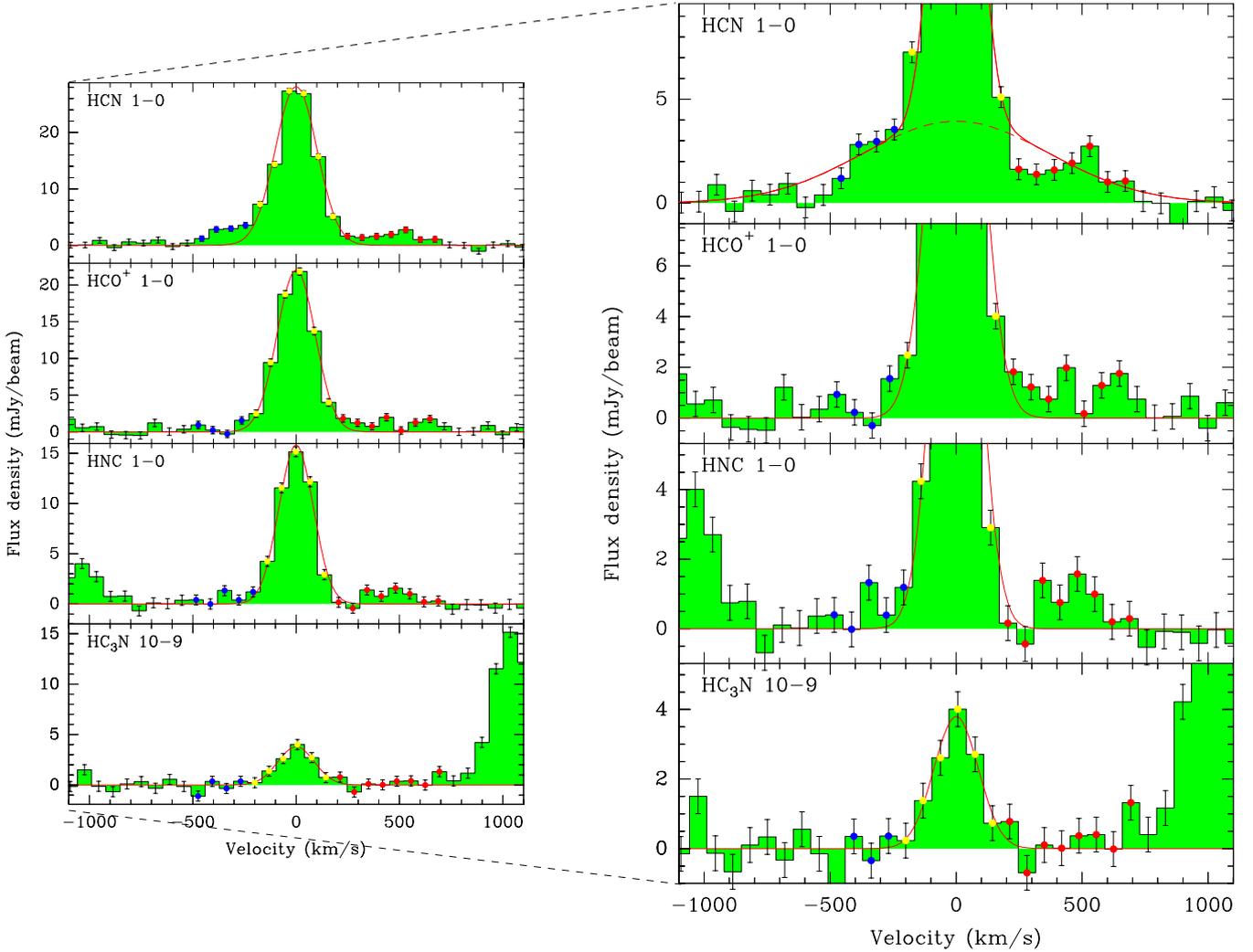
Fig. 1. Plateau de Bure spectra of HCN, HCO⁺, HNC 1–0 and HC₃N 10–9. In *the right panels* we have zoomed-in on the base of the line to show the line wings more clearly. In general, red solid lines show Gaussian fits to the line center (core) line widths and are 197 km s⁻¹ for HC₃N and HNC, 213 km s⁻¹ for HCO⁺ and 236 km s⁻¹ for HCN. However, in *the top right panel* of HCN 1–0 we instead show two Gaussian fits (one with $\delta V(FWHM) = 180$ km s⁻¹ and one with $\delta V(FWHM) = 870$ km s⁻¹), as discussed in Sect. 3.1. Zero velocity was set for redshift $z = 0.042170$.

by the peak position of the integrated HCN 1–0 emission (see Fig. 3). Given the positional uncertainties, we may conclude that the wings have their peak brightness within 0.5 kpc of the nucleus. Furthermore, a faint blue-shifted wing feature can be seen tentatively 2″ to the west of the nucleus (a similar feature is seen around the systemic velocity). Faint red-shifted wing emission is curving out 2″ northeast of the center. These features should be confirmed at higher sensitivity.

3.2. HCO⁺, HNC, and HC₃N

In the HCO⁺ and HNC spectra (see Fig. 1 and Table 1) the wings can also be seen – although they are weaker than for HCN. The peak ($V = 0$ km s⁻¹) line intensity ratio between HCN and HCO⁺ is 1.3, while the ratio in the wings (summed from +200 to +700 km s⁻¹ and from –200 to –700 km s⁻¹) is ≈2.2. For comparison, the integrated line ratio is reported to be ≈1.8 in the single-dish survey of Costagliola et al. (2011). The peak HCN/HNC line intensity ratio is 1.8 and the line wing ratio is ≈2.8. For comparison, the integrated line HCN/HNC ratio is ≈2.6 in the single-dish survey of Costagliola et al. (2011). The rotation of the main disk is evident for both HCO⁺ and HNC (see Fig. 7).

The line center integrated intensity maps of HCO⁺ and HNC are presented in Fig. 6.

Emission from the HC₃N molecule is found for the first time in Mrk 231 through the detection of the HC₃N $J = 10–9$ line (see Fig. 6). Its line width is similar (≈197 km s⁻¹) to that of the HNC line center. The HCN 1–0/HC₃N 10–9 peak line ratio is 7.7 (in the Costagliola et al. (2011) single-dish survey a lower limit of 14 is found). The HC₃N 10–9 emission is unresolved in the 1″55 × 1″28 beam.

4. Discussion

4.1. The extent of the HCN line wings

We confirm the result of Feruglio et al. (2010) that the line wings are emerging from a spatially extended structure. This supports the notion that they originate in an extended outflow – rather than representing the extremes of a Keplerian nuclear disk. (The notion of extended Keplerian rotation fails on the extreme required enclosed mass.) A two-dimensional Gaussian fit to the integrated intensity map of the red-shifted wing results in a full-width-at-half-maximum (*FWHM*) size of 0″85 ± 0″2 (1″ = 870 pc). The corresponding map for the blue-shifted wing has
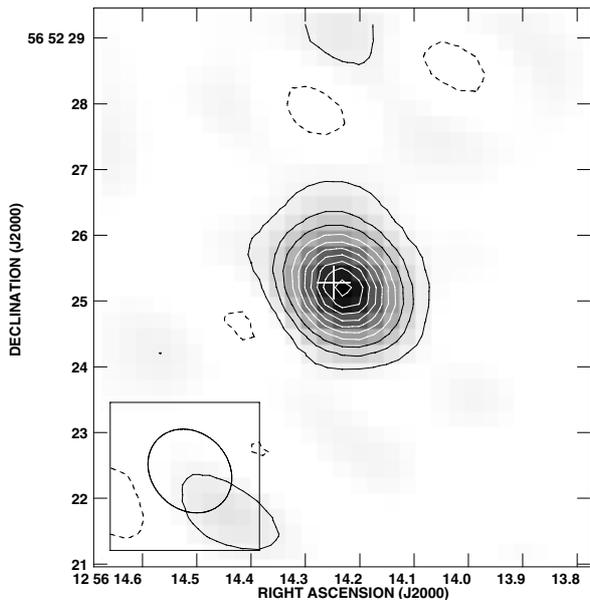
Fig. 2. 85 GHz continuum image of Mrk 231, the VLBI position is marked with a cross (see footnote to Table 1). Ellipse indicates beam size and orientation.

lower signal-to-noise and a Gaussian fits results in a *FWHM* size of $0\farcs75 \pm 0\farcs3$.

Comparing the HCN and HCO$^+$ wings with the structure of the atomic (neutral) gas as seen in absorption (Rupke & Veilleux 2011), the results are consistent with an almost face-on nuclear wind. Rupke & Veilleux (2011) find the most highly accelerated atomic gas in the northern region (with peak velocities occurring around $2\farcs3$ (2 kpc) north of the nucleus) where the radio jet is interacting with the neutral material. Rupke & Veilleux (2011) suggest that the jet is entraining material from the large-scale wind that accelerates it even more which is a phenomenon seen also in other AGNs (Matsushita et al. 2007). There is a hint of this feature at the $1.5 - 2\sigma$ level in our HCN integrated intensity map of the red-shifted wind – but this requires confirmation at higher sensitivity. Furthermore, the velocities of the nuclear wind described by Rupke & Veilleux (2011) and the HCN wings generally agree well. The molecular HCN wings we find occur equally close (possibly even closer) to the nucleus as the atomic wind. We find no correspondence to the starburst wind found $3''$ south of the nucleus by Rupke & Veilleux (2011) and we conclude that the HCN wings originate in the nuclear wind, as does the atomic wind.

4.2. Why is the HCN emission enhanced in the line wings?

The CO 1–0 wing peak intensity is 8 mJy (Feruglio et al. 2010) and for HCN 1–0 it is 3 mJy. For the same source size – and transferring to temperature scale – the $T_B(CO)/T_B(HCN)$ 1–0 ratio in the wings is 1.6 – which is lower than for the line peak at center velocity. This is either because the outflowing molecular gas is dense, with elevated HCN abundances, or it is caused by mid-IR pumping of HCN.

4.2.1. Dense molecular gas in the outflow

If we assume that the HCN molecule is collisionally excited, the density in the outflow has to be at least $n = 10^4$ cm^{-3} for the line to begin to be excited, even if the HCN abundance is enhanced.

We can use a simple non-LTE RADEX (van der Tak et al. 2007) model to investigate the CO/HCN 1–0 line ratios in a few possible scenarios. The models are not unique and serve only as illustrations of possibilities. (Note also that without multi-transition HCN information we are unable to constrain the properties of the dense gas in the outflow.)

We adopt a temperature of the outflowing gas of $T_k = 100$ K (the lowest gas temperature fit of González-Alfonso et al. (2010) from *Herschel* observations of the molecular gas of Mrk 231) and note that for densities $n = 10^4$ cm^{-3} solutions require an HCN abundance (relative to H$_2$) of $X(HCN) \gtrsim 10^{-6}$. It is actually the relative CO and HCN column densities that are constrained by RADEX – this means that we have to assume a standard CO to H$_2$ abundance ratio (in this case of 10^{-4}) to obtain the HCN abundance $X(HCN)$. Such an HCN abundance would be considered very high (but see Sect. 4.2.2 below for a brief discussion). For a number density $n = 10^5$ cm^{-3} a line ratio between CO and HCN 1–0 of 2 can be achieved for optically thin ($\tau < 1$) CO and HCN with a column density ratio ($N(HCN)/N(CO)$) of 5×10^{-4}. If we assume a CO abundance of 10^{-4} (relative to H$_2$), this would imply an HCN abundance of $X(HCN) = 5 \times 10^{-8}$, which is high – but not unusually so (see Sect. 4.2.2 below). Intrinsic brightness temperatures for optically thin emission would be low, however, and the emission would have to have a large filling factor. The low HCN/H^{13}CN 1–0 intensity ratio of 5.5 observed by Costagliola et al. (2011) suggests that the HCN 1–0 emission towards Mrk 231 is not optically thin. This is a global ratio, however, and the ratio for the wing component is difficult to determine.

A low intensity ratio between CO and HCN can also be achieved by a clumpy outflow where the individual clumps are dense and optically thick. A $T_B(CO)/T_B(HCN)$ ratio of ≈ 2 can be obtained for a range of abundances depending on how high the CO column density can become in each clump. If we avoid the most extreme optical depths in CO, then HCN abundances of $X(HCN) = 10^{-8}-10^{-7}$ will fit the observed line ratio. This scenario (or the optically thin one above) does not allow any CO 1–0 emission to emerge from a diffuse, low-density ($n = 10^2-10^3$ cm^{-3}) component in the outflow – such a component would only contribute to the CO 1–0 luminosity, not the HCN. Therefore, if the molecules are collisionally excited, the low intensity ratio between CO and HCN in the outflow leaves little room for a low-density molecular component.

4.2.2. Outflow abundances

HCN abundances: elevated HCN abundances have been observed in outflows in the Galaxy. For example, HCN abundances of 14×10^{-8} are found in the outflow lobes of regions of massive star-formation (e.g. Su et al. 2007; Liu et al. 2011). The fact that the outflow in Mrk 231 is seen (tentatively) in H$_2$O absorption (González-Alfonso et al. 2010) may suggest that shocks are involved in removing the water from the grains. Are we seeing indications of HCN abundances being enhanced in the shocks of the outflow? Evidence that this can be the case are presented by Tafalla et al. (2010). They argue that HCN is mainly produced in shocks by the reaction of N with CH$_2$ – where CH$_2$ is formed in the reaction between C and H$_3^+$ or C$^+$ with H$_2$. Thus, for HCN to be selectively produced in the shock, a sufficient abundance of free C is required. SiO emission from shocks in galaxy-scale outflows has been observed in the starburst wind of M 82 (García-Burillo et al. 2001) and may also be expected to be elevated in the Mrk 231 outflow.
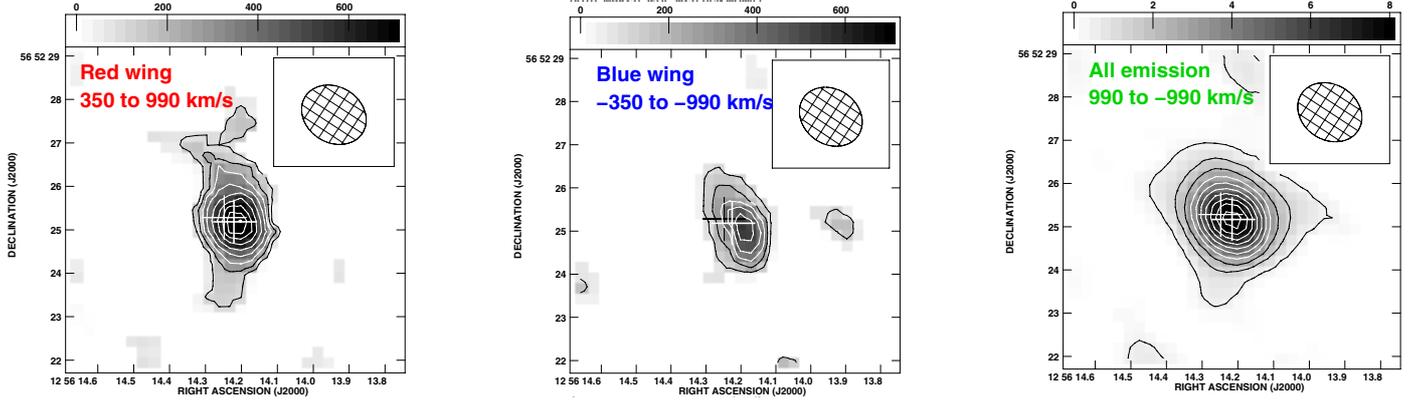
Fig. 3. Integrated intensities of the HCN 1–0 line emission. *Left panel*: the red-shifted wing emission from 350 to 990 km s⁻¹. The grayscale range is from 0 to 0.7 Jy km s⁻¹ (beam)⁻¹ and the contours start at 0.098 Jy km s⁻¹ (beam)⁻¹ with steps of 0.0998 Jy km s⁻¹ (beam)⁻¹. *Middle panel*: the blue-shifted wing emission from −990 to −350 km s⁻¹. Same grayscale and contours as for the previous panel. *Right panel*: the total (from −990 km s⁻¹ to 990 km s⁻¹) integrated HCN 1–0 line emission from Mrk 231. The grayscale range is from 0 to 8 Jy km s⁻¹ (beam)⁻¹ and the contour levels are 0.45 Jy km s⁻¹ (beam)⁻¹ × (1,3,5,7,9,11,13,15,17,19). The thick white crosses mark the peak of the integrated HCN 1–0 line emission and the thinner crosses indicate the VLBI position (see footnote to Table 1) and 1″ = 870 pc. Hatched ellipse indicates beam size and orientation.
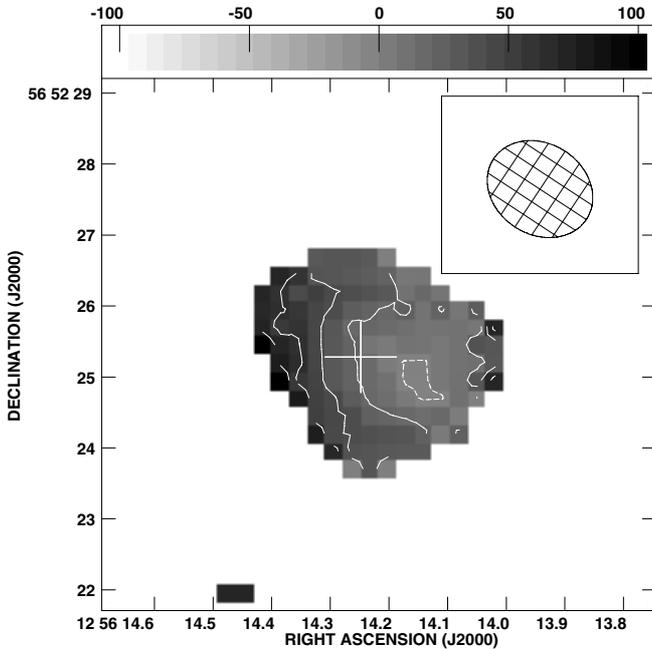
Fig. 4. HCN 1–0 velocity field (including only velocities ±200 km s⁻¹) showing the rotation of the molecular disk. The HCN 1–0 emission rotates in the same east-west fashion as the ¹²CO emission (Bryant & Scoville 1996; Downes & Solomon 1998). The grayscale ranges from −100 to 100 km s⁻¹ and the contours are 20 km s⁻¹ × (−4, −3, −2, −1, 0, 1, 2, 3, 4). Zero velocity was set to redshift $z = 0.042170$ and 1″ = 870 pc. Cross marks the VLBI radio continuum position (see footnote to Table 1). Hatched ellipse indicates beam size and orientation.

Note also that a large HCN abundance is a general result of high temperatures. Harada et al. (2010) have shown that HCN abundances may reach 10^{-6} in regions where $T \gtrsim 300$ K. They also find enhancements of H_2O abundances in their high-temperature models – therefore HCN and H_2O abundance enhancements may be a result of high temperatures and not specifically shock chemistry. A potential scenario is that the molecular abundances reflect the high temperatures near the AGN and retain these abundances in the outflow. However, without

Table 1. Line flux densities[a].

| Line	Peak	Wing[b]	Integrated
	[mJy beam⁻¹]	[mJy beam⁻¹]	[Jy km s⁻¹]
HCN 1–0	28 ± 0.5	3	8.4
HCO⁺ 1–0	22 ± 0.5	2	5.6
HNC 1–0	15 ± 0.5	1	3.7
HC₃N	3 ± 0.5	. . .	0.9

Notes. [a] The 3 mm continuum position is α: 12:56:14.230 ± 0.0013 δ: 56:52:25.206 ± 0.01 (J2000). A Gaussian fit to the continuum source gives a flux density of 25.0 ± 0.6 mJy and an upper limit to the source size of 0″.39. The VLBI radio continuum peak is: α: 12:56:14.248 δ: 56:52:25.28 (J2000) (Carilli et al. 1998). [b] From the red-shifted wing at $V = +500$ km s⁻¹.

a source of heating, the outflowing gas will cool very quickly if it remains at high density and potential ion-neutral reactions (involving e.g. H^+, H_2^+, O^+, H_3O^+ etc.) may destroy HCN on short time-scales. So it is unclear whether the gas can retain relic high-temperature abundances of HCN. Furthermore, at least part of the outflow will be exposed to the X-rays of the nuclear AGN, which means that it could possibly influence the chemistry of the outflowing gas (e.g. Maloney et al. 1996; Meijerink & Spaans 2005; Meijerink et al. 2006).

HNC and HCO⁺ abundances: the HCN intensity is greater than that of HCO⁺ by a factor of two in the line wings. This could be caused by excitation or by HCN being more abundant than HCO⁺. In Galactic outflow sources, $I(\text{HCN}) > I(\text{HCO}^+)$ (and abundance ratios HCN/HCO⁺ = 10–50) are not uncommon (Tafalla et al. 2010) and may simply be a result of the enhanced HCN abundance in the outflow due to shocks and high temperatures. The line wing HCN/HNC ratio of 2.8 is within the range of what is typically observed in galaxies (e.g. Costagliola et al. 2011). In general HNC is expected to be destroyed in shocks – and at high temperatures (e.g. Schilke et al. 1992). For the second model in Sect. 4.2 an abundance ratio HCN/HNC and HCN/HCO⁺ of ≈20 may reproduce the observed 1–0 line ratios in the line wings. Both these abundance ratios are consistent with values found for Galactic shock regions.
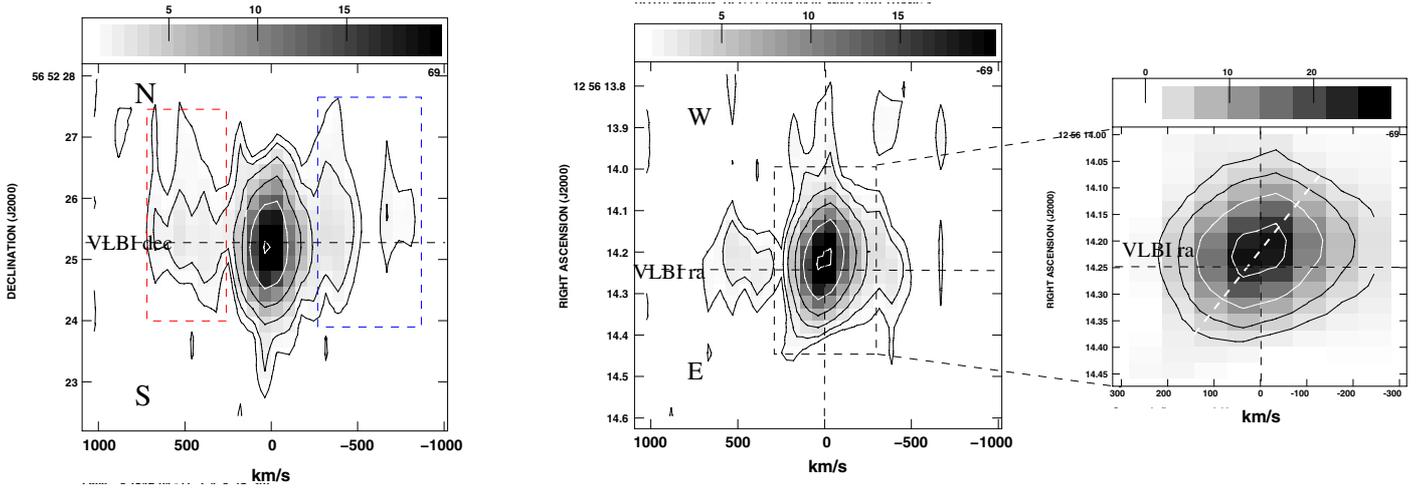
Fig. 5. HCN 1–0 position-velocity (pV) diagrams. *Left*: north-south cut along the minor axis of the disk rotation. The extended nature of the line wings is evident here. *Center*: east-west cut (along the major axis of the rotating disk) and *Right*: zoom-in on the disk rotation (1″ = 870 pc).
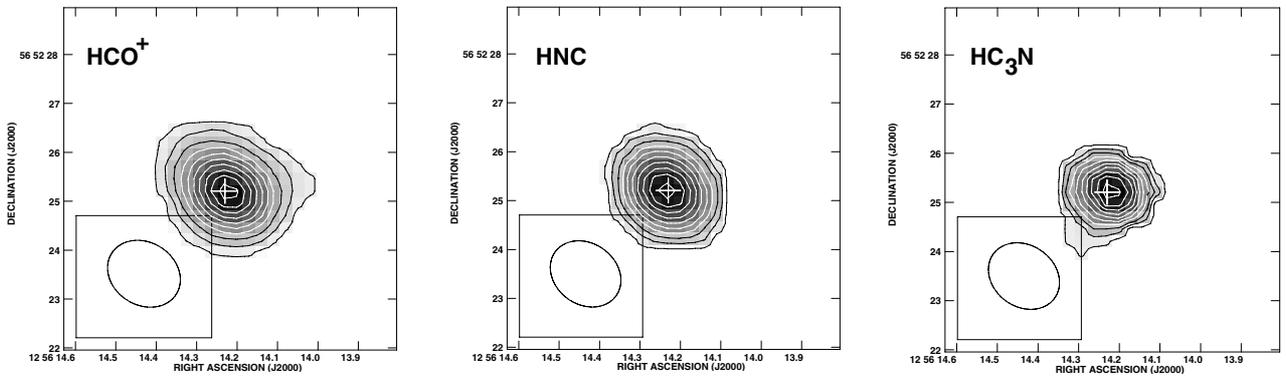
Fig. 6. Integrated intensities (from *left to right*) of the HCO⁺, HNC 1–0 and HC₃N 10–9 line emission. The grayscale range is from 0 to 5.3, 0 to 3.3, and 0 to 1.0 Jy km s^{-1} (beam)$^{-1}$ respectively. The contour levels are 0.26, 0.16, and 0.04 Jy km s^{-1} (beam)$^{-1}$ × (1,3,5,7,9,11,13,15,17,19). (1″ = 870 pc and and zero velocity was set to redshift $z = 0.042170$ for all lines). Cross refers to the center of the 85 GHz continuum. The maps are integrated over ±200 km s^{-1} and exclude the line wings. Ellipse indicates beam size and orientation.

4.2.3. IR pumping

An alternative scenario to collisional excitation of HCN is pumping by 14 μm mid-IR continuum. The rotational levels are then populated via the IR bending modes. Vibrational line emission from HCN has been observed in ULIRGs such as Arp 220 (Salter et al. 2008) and in LIRGs like NGC 4418 (Sakamoto et al. 2010), showing that the HCN molecule is pumped by mid-IR absorption in these galaxies. For HCN to be pumped a minimum 14 μm brightness temperature of $T_{\rm B}({\rm IR}) = 85$ K is required (e.g. Aalto et al. 2007). If IR pumping dominates the HCN excitation no dense clumps in the outflow are needed to explain the HCN emission. It is therefore important to settle the question of the excitation of HCN in the outflow. Furthermore, both HCO⁺ and HNC may be pumped by mid-IR emission (Aalto et al. 2007) through bending modes in the same way as for HCN. HNC is pumped already at 21 μm and HCO⁺ at 12 μm.

In the SED for Mrk 231 (González-Alfonso et al. 2010) the 14 μm regime is dominated by a hot component with $T_{\rm d} = 150$–400 K emerging from the inner 40–50 pc. One would expect the strongest pumping of HCN close to this hot component, i.e., the nucleus. Furthermore, the plane of the disk is likely opaque at 14 μm, but the gas lifted out of the plane in the outflow will have an unobstructed view of the nuclear region. Very tentatively, one

might argue therefore that the HCN in the wings is pumped more strongly than that in the core of the line. However, the extended nature of the wings implies that the gas is at least a few hundred pc from the IR source and the resulting brightness temperature produced by this source is going to be well below 85 K, rendering the pumping scenario unlikely. This argument holds also for HNC and HCO⁺.

It is interesting to compare the potential HCN pumping scenario to the case for water detected by Herschel (González-Alfonso et al. 2010). H₂O is pumped at significantly longer wavelengths (than HCN) from 45 to 75 μm and may therefore be pumped by the warm, more extended dust component ($r = 120$ pc disk with $T_{\rm d} = 95$ K, González-Alfonso et al. 2010). This region is smaller than that of the HCN line wings and the H₂O absorption line profile also appears different from that of the HCN line wings. It is therefore possible that H₂O is IR-pumped while HCN is not.

4.3. Gas properties and the nature of the outflow

Our interpretation of the HCN-luminous wings of Mrk 231 is that the molecular gas in the outflow is clumpy and dense, with an enhanced HCN abundance. The similar spectral shapes (and
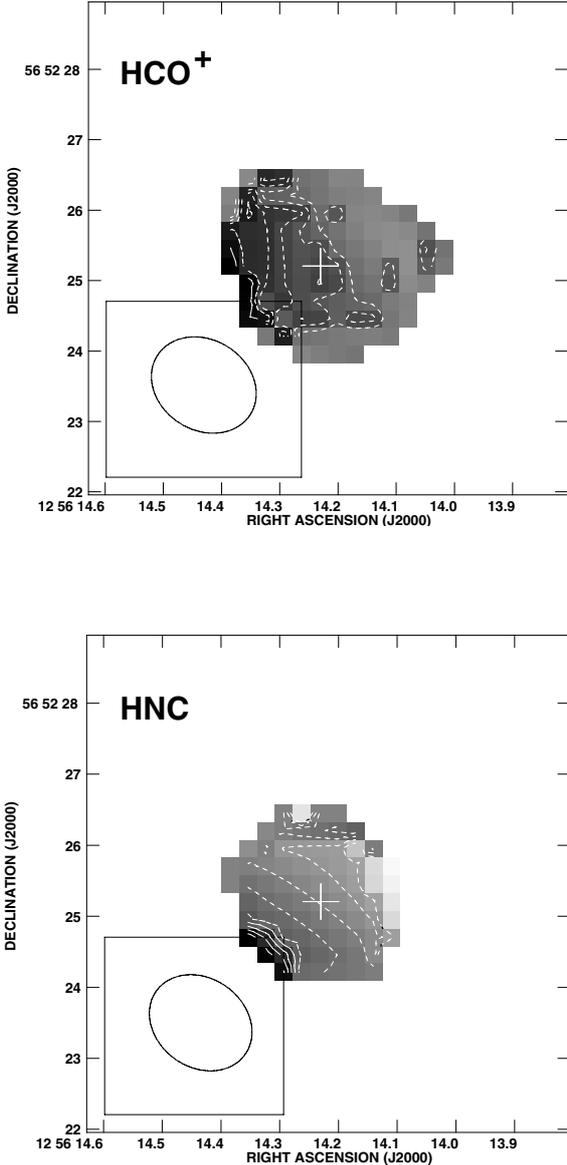
Fig. 7. Central HCO⁺ (*top*) and HNC (*bottom*) 1–0 velocity fields. The grayscale range is from −64 to 9 km s⁻¹ (top) and from −43 to 24 km s⁻¹ (bottom). The contour levels are 5 km s⁻¹ × (−4, −3, −2, −1, 0, 1, 2, 3, 4). (1″ = 870 pc and zero velocity was set to redshift z = 0.042170 for all lines). Cross refers to the center of the 85 GHz continuum. The emission is integrated over ±200 km s⁻¹ and excludes the line wings. Ellipse indicates beam size and orientation.

spatial extent within the errors) of the CO and HCN 1–0 line wings suggest that the emission is emerging from the same outflowing gas. This would then imply that there is no significant evolution (e.g. star-formation or evaporation) of the cloud properties along the molecular part of the outflow. This is inconsistent with the simulations of molecular cloud properties entrained in outflows by Narayanan et al. (2008), who predict a shorter lifetime and smaller spatial extent of the dense gas phase – as well as ongoing star-formation in the outflowing molecular gas. The Mrk 231 molecular outflow appears instead to be dominated by the dense phase without much low-density molecular gas. Is this because radiation dissociates the low-density gas, or because it becomes compressed in the flow? Alternatively, the molecular cloud structure largely reflects the interstellar medium structure from where it becomes launched into the outflow. Note that the

spatial extent of the CO and HCN wings must be better determined for a deeper exploration of the evolution of the gas in the outflow.

In an AGN-driven outflow, the molecular gas can be entrained by a thermal hot wind or driven by momentum deposition. Rupke & Veilleux (2011) find that the neutral gas has higher velocities than the ionized gas in Mrk 231, which is not consistent with entrainment by a hot wind. They suggest the AGN-driven two-phase model by Hopkins & Elvis (2010) as a possible scenario for the neutral wind of Mrk 231: close to the center, the AGN acts on the hot interstellar medium, powering an outflow that causes the cold molecular clouds to expand, which makes them more susceptible to being carried outward by radiation pressure (and to become ionized). However, this requires a mechanism to rapidly compress the molecular gas in the subsequent radiation pressure-driven wind for it to be consistent with our observations. Alternatively, radiation pressure-driven outflows could be launched directly, close to the black hole (e.g. King 2003). Dense molecular gas from the inner regions of Mrk 231 may then be compressed even more in the outflow without being initially disrupted. High HCN abundances may indicate shock enrichment in the outflow and/or that the chemistry is influenced by the AGN. It is interesting to speculate if HCN-luminous wings may be a general signature of AGN-driven outflows in luminous galaxies. High-sensitivity HCN surveys of starburst and AGN-driven outflows will provide us with an answer.

We note that Chung et al. (2011) detected CN emission only toward the AGN-driven objects, in their stacked survey of outflows in ULIRGs, not toward the starbursts. This is either because of higher gas densities in these outflows, or because of CN abundance enhancements, and also emphasizes the importance of studying the molecular gas properties of outflowing AGN and starburst galaxies.

4.4. Serendipitous HC₃N detection: warm, shielded gas in the nucleus.

The fitted upper size limit of the HC₃N 10–9 integrated line emission is $FWHM$ = 0″.48 (400 pc) and it is centered on the nucleus of Mrk 231. Emission is not detected in the line wings. The peak-to-peak line ratio between HC₃N 10–9 and HCN 1–0 is 0.14 ± 0.015 – which makes the HC₃N line emission (relative to HCN) brighter than in, for example, NGC 1068 or NGC 7771 – and almost as bright as in Arp 220 (Costagliola et al. 2011). Models by Harada & Herbst (2010) indicate that HC₃N abundances may be enhanced substantially (orders of magnitude) in warm (>200 K) regions in the midplane of dense disks around AGNs. These regions do not qualify as XDRs – X-ray dominated regions – but may be buried within the XDR. According to models based on the recent Herschel observations (van der Werf et al. 2010), the gas in the 1.1 kpc starburst disk is exposed to intense UV emission – which should effectively destroy the HC₃N molecules. Since the size of the HC₃N emitting region is smaller than the suggested dimensions of the starburst disk, the HC₃N emission may emerge from a region between the inner edge of the starburst disk and the AGN dominated XDR. In the dust SED model by González-Alfonso et al. (2010) the nuclear hot component with T_d = 150−400 K originates in the inner 40–50 pc. This may therefore be the location from where the HC₃N is emerging – consistent with the expected HC₃N abundance enhancement in warm, dusty regions. The high bulk temperature required for significant abundance enhancement is consistent with the AGN as the heating agent. It is possible that this

dusty, warm region represents the final stage of the obscured, X-ray absorbed (e.g. Page et al. 2004) accretion phase of the QSO.

4.5. Future outlook

We have seen that the molecular outflow in Mrk 231 has surprising gas properties and physical conditions that contain important clues to its origin, physical conditions, and chemical composition. To fully understand the enhancement of HCN (and also the HCO$^+$ and HNC emission), multi-transition, high-resolution observations are necessary. Other species such as multi-line CO observations, isotopic variants of CO, HCN, HCO$^+$ and HNC, shock tracers like SiO and CH$_3$OH will provide essential, new pieces to this puzzle. These studies should be accompanied by radiative transport and astrochemical modeling. Deep imaging of CO and HCN will test the notion that the emission is co-spatial and originates in the same gas.

The detection of HC$_3$N emission toward the inner region of Mrk 231 raises interesting questions about regions of shielded gas near the nucleus of this ULIRG QSO. High-resolution observations will pinpoint the exact location of the HC$_3$N emitting regions, allowing us to better understand the underlying mechanisms and evolution of this powerful galaxy.

5. Conclusions

In this paper we present the first high-resolution observations of HCN, HCO$^+$ and HNC 1–0 emission from the wings of the prominent molecular outflow of the QSO ULIRG Mrk 231. The velocities (≈ 750 km s^{-1}) are similar to those already found for the CO-outflow. The line wings are spatially extended by at least $0\farcs75$ (>700 pc) in a north-south direction. This is the first time prominent HCN and HCO$^+$ emission has been detected in a large-scale galactic outflow. The east-west rotation of the main disk is also evident in the HCN, HCO$^+$ and HNC 1–0 narrow component line emission.

Compared to CO 1–0, HCN 1–0 appears relatively enhanced in the line wings by factors of 2–5. This suggests that a large fraction of the gas in the outflow is dense $n > 10^4$ cm^{-3}, which is consistent with the molecular gas being compressed and fragmented by shocks. The HCN abundances may be significantly elevated ($X(\text{HCN}) > 10^{-8}$) in the outflow, which can be caused by shocks and/or high temperature chemistry.

Alternatively, the excitation of HCN could be affected by mid-IR radiation, but we suggest that this is less likely because of the extended nature of the outflow.

The HCN/HCO$^+$ line peak ratio is 1.3 for the line center and 2.2 in the line wings. I(HCN)>I(HCO$^+$) is not uncommon in outflowing gas in Galactic sources. The peak center HCN/HNC line ratio is 1.8 and the line wing ratio is 2.8. This is within the range of what is typically observed in galaxies.

An unexpectedly bright HC$_3$N 10–9 line was detected in the central 400 pc of Mrk 231. This molecule is often associated with young star-forming regions and tends to be destroyed by intense UV and particle radiation. We find it unlikely that the emission originates in the starburst region of Mrk 231 and instead

suggest that the HC$_3$N emission is emerging from a shielded, dust-enshrouded region within the inner 40–50 pc where the gas is heated to high temperatures (200–300 K) by the AGN. We speculate that this dusty, warm region represens the final stage of the obscured, X-ray absorbed accretion phase of the QSO in Mrk 231.

References

Aalto, S., Spaans, M., Wiedner, M. C., & Hüttemeister, S. 2007, A&A, 464, 193
Alatalo, K., Blitz, L., Young, L. M., et al. 2011, ApJ, 735, 88
Baan, W. A. 2007, New A Rev., 51, 149
Bryant, P. M., & Scoville, N. Z. 1996, ApJ, 457, 678
Carilli, C. L., Wrobel, J. M., & Ulvestad, J. S. 1998, AJ, 115, 928
Chung, A., Yun, M. S., Naraynan, G., Heyer, M., & Erickson, N. R. 2011, ApJ, 732, L15
Costagliola, F., Aalto, S., Rodriguez, M. I., et al. 2011, A&A, 528, A30
Downes, D., & Solomon, P. M. 1998, ApJ, 507, 615
Feruglio, C., Maiolino, R., Piconcelli, E., et al. 2010, A&A, 518, L155
Fischer, J., Sturm, E., González-Alfonso, E., et al. 2010, A&A, 518, L41
Gallagher, S. C., Brandt, W. N., Chartas, G., Garmire, G. P., & Sambruna, R. M. 2002, ApJ, 569, 655
García-Burillo, S., Martín-Pintado, J., Fuente, A., & Neri, R. 2001, ApJ, 563, L27
González-Alfonso, E., Fischer, J., Isaak, K., et al. 2010, A&A, 518, L43
Harada, N., & Herbst, E. 2010, in 65th International Symposium On Molecular Spectroscopy
Harada, N., Herbst, E., & Wakelam, V. 2010, ApJ, 721, 1570
Hopkins, P. F., & Elvis, M. 2010, MNRAS, 401, 7
Hopkins, P. F., Bundy, K., Murray, N., et al. 2009, MNRAS, 398, 898
King, A. 2003, ApJ, 596, L27
Lipari, S., Sanchez, S. F., Bergmann, M., et al. 2009, MNRAS, 392, 1295
Liu, T., Wu, Y., Liu, S.-Y., et al. 2011, ApJ, 730, 102
Lonsdale, C. J., Lonsdale, C. J., Smith, H. E., & Diamond, P. J. 2003, ApJ, 592, 804
Maloney, P. R., Hollenbach, D. J., & Tielens, A. G. G. M. 1996, ApJ, 466, 561
Matsushita, S., Muller, S., & Lim, J. 2007, A&A, 468, L49
Meijerink, R., & Spaans, M. 2005, A&A, 436, 397
Meijerink, R., Spaans, M., & Israel, F. P. 2006, ApJ, 650, L103
Murray, N., Quataert, E., & Thompson, T. A. 2005, ApJ, 618, 569
Nakai, N., Hayashi, M., Handa, T., et al. 1987, PASJ, 39, 685
Narayanan, D., Cox, T. J., Kelly, B., et al. 2008, ApJS, 176, 331
Page, M. J., Stevens, J. A., Ivison, R. J., & Carrera, F. J. 2004, ApJ, 611, L85
Rupke, D. S. N., & Veilleux, S. 2011, ApJ, 729, L27
Sakamoto, K., Aalto, S., Evans, A. S., Wiedner, M. C., & Wilner, D. J. 2010, ApJ, 725, L228
Sakamoto, K., Ho, P. T. P., & Peck, A. B. 2006, ApJ, 644, 862
Salter, C. J., Ghosh, T., Catinella, B., et al. 2008, AJ, 136, 389
Schilke, P., Walmsley, C. M., Pineau Des Forets, G., et al. 1992, A&A, 256, 595
Sturm, E., González-Alfonso, E., Veilleux, S., et al. 2011, ApJ, 733, L16
Su, Y.-N., Liu, S.-Y., Chen, H.-R., Zhang, Q., & Cesaroni, R. 2007, ApJ, 671, 571
Tafalla, M., Santiago-García, J., Hacar, A., & Bachiller, R. 2010, A&A, 522, A91
Taylor, G. B., Silver, C. S., Ulvestad, J. S., & Carilli, C. L. 1999, ApJ, 519, 185
van der Tak, F. F. S., Black, J. H., Schöier, F. L., Jansen, D. J., & van Dishoeck, E. F. 2007, A&A, 468, 627
van der Werf, P. P., Isaak, K. G., Meijerink, R., et al. 2010, A&A, 518, L42
Walter, F., Weiss, A., & Scoville, N. 2002, ApJ, 580, L21
Wilson, C. D., Petitpas, G. R., Iono, D., et al. 2008, ApJS, 178, 189